J Supercond Nov Magn (2017) 30:1137–1143
DOI 10.1007/s10948-016-3891-6

ORIGINAL PAPER

# Microstructures Property and Improved $J_c$ of Eu-Doped $YBa_2Cu_{3.6}O_{7-\delta}$ Thin Films by Trifluoroacetate Metal Organic Deposition Process

**MY Li[1] · Q Fang[1] · XF Hu[1] · ZY Liu[1,2] · YQ Guo[1,2] · YM Lu[1,2] · CY Bai[1,2] · CB Cai[1,2]**

Received: 21 August 2016 / Accepted: 27 October 2016 / Published online: 28 November 2016


**Abstract** $YEu_xBa_2Cu_{3.6}O_{7-\delta}$(x = 0, 0.1, 0.3, 0.5) thin films were prepared on buffered substrates by trifluoroacetate metal organic deposition (TFA-MOD). The europium-doped film showed better out- and in-plane texture than the pure $YBa_2Cu_{3.6}O_{7-\delta}$ thin film and special topography. In the meantime, the superconducting transition temperature $T_c$ was improved with the increase of europium content and spanned a small range when $x = 0.5$ doping levels. Besides, the $J_c$ value was obviously enhanced with europium addition, and $YEu_{0.3}Ba_2Cu_{3.6}O_{7-\delta}$ showed the best superconducting properties under self-field. Furthermore, the $J_c$ value was obviously improved under magnetic field, and the enhanced flux-pinning properties was also observed in europium-substituted samples which may be attributed to the good grain connections and the effective flux pinning centers introduced by europium addition. The thickness of prepared film samples were approximately 400 nm. The structure of samples were characterized by x-ray diffraction (XRD), Raman spectrum was used to investigate the crystallization and growth orientation, and the surface morphology of films were got by field-emission scanning electronic microscopy (FE-SEM). Moreover, energydispersive spectroscopy (EDS) was utilized to determine element composition. Spatial distribution of $J_c$ of the film was obtained by mapping analysis of inductive measurement at 77 K. And the superconducting properties under magnetic fields were measured by magnetic property measurement system with a SQUID magnetometer.

**Keywords** Critical current density · Europium addition · Flux pinning · TFA-MOD · Microstructures · Superconducting transition temperature

## 1 Introduction

$YBa_2Cu_3O_{7-\delta}$ coated conductors (CCs) are high-current conductors that display outstanding performances in the respect of temperature and magnetic field and the most promising materials for motors, generators, transformers, and superconducting magnetic energy storage systems and so on [1, 2]. However, the low-current densities with increasing the magnetic fields and temperatures prevent the large-scale applications of CCs. Many great breakthroughs in the CCs research have been achieved recently [3–5]. These results have illustrated that introduction of proper artificial flux pinning centers can distinctly improve the current carrying capabilities of CCs. Among these present techniques, the critical strategies to enhance $J_c$ mainly include substrate surface decoration [6–8], impurity addition [9–11], rare earth (RE) addition or substitution [12–15], and combined methods [6]. Among these strategies, RE addition is one of the most promising approaches for its valuable advantages such as high efficiency and easy control. $REBa_2Cu_3O_{7-x}$ (RE: Nd, Sm, Gd, and Er) films had been studied [6, 14, 16], which led to improvement in the in-magnetic-field current density of the conductor. Moreover, it is reported that the addition of $RE_2O_3$ (RE: Y, Dy, and Ho) can also produce nanoparticles with a size range of 10–50 nm and enhance the flux pinning properties [17, 18].

✉ CB Cai
cbcai@t.shu.edu.cn

[1] Shanghai Key Laboratory of High Temperature Superconductors, Physics Department, Shanghai University, 99 Shangda Road, Shanghai 200444, China

[2] Shanghai Creative Superconductor Technologies Co. Ltd, Shanghai 201401, China

Among various technologies used for the deposition of REBCO films, trifluoroacetate metal organic deposition (TFA-MOD) has several advantages such as low cost, epitaxial growth applicability, precise controllability of the chemical composition, and easy application to large substrates. And recently, the optimization for the TFA-MOD method to prepare yttrium barium copper oxide (YBCO) CCs has spurred its commercialization. However, the complex reaction process of TFA-MOD requires precisely controlled parameters to achieve high-performance YBCO films [19]. Some reports determined the complete decomposition reaction by the released gases during metal–trifluoroacetate thermal decomposition [20]. Although the chemical reaction path prior to high-performance pure YBCO nucleation has been extensively studied, many details of the process are still unclear. Especially when high-performance YBCO films are prepared by impurity addition using TF-MOD process, the precursor evolution of nanoparticles of this process is still an open question. The knowledge of the precursor evolution is essential for the YBCO-coated conductors with competitive superconducting performance.

In this work, YBCO superconductor films with europium (Eu) addition were successfully prepared on buffer layer substrates by a TFA-MOD process, whose $J_c$ can reach 2.52 MA/cm$^2$ (77 K, 0 T). We also carefully investigated the flux pinning characteristics of Eu-doped YBCO film through a comparative study with the pure YBCO film. In addition, a preliminary analysis of the growth mechanism of the doped film was carried out.

## 2 Experimental

$YEu_xBa_2Cu_{3.6}O_{7-\delta}$(x = 0, 0.1, 0.3, 0.5) thin films were prepared on buffered substrates by TFA-MOD. Y, Eu, and Cu acetates were dissolved into propionic acid and deionized water, the atomic ratio of the element Y and Eu equals to 1:0.1, 1:0.3 and 1:0.5 Ba acetates were dissolved into trifluoroacetic acid and deionized water, and the solutions were stirred for 2 h at room temperature. Then, the solutions were refined by distillation process to yield blue glassy residues, and the blue glassy residues would be dissolved into methanol. The solutions were refined for three times in order to remove water, TFA, and propionic and acetic acid impurities. Finally, methanol was added into the solutions to adjust the solution concentration to 2.5 mol/L

All thin films were prepared on hast/$Al_2O_3$/$Y_2O_3$/IBAD-MgO/Epi-MgO/LMO buffer layer substrates by dip coating method. Then the precursor films were put into a hightemperature tube furnace for pyrolysis treatment, which was

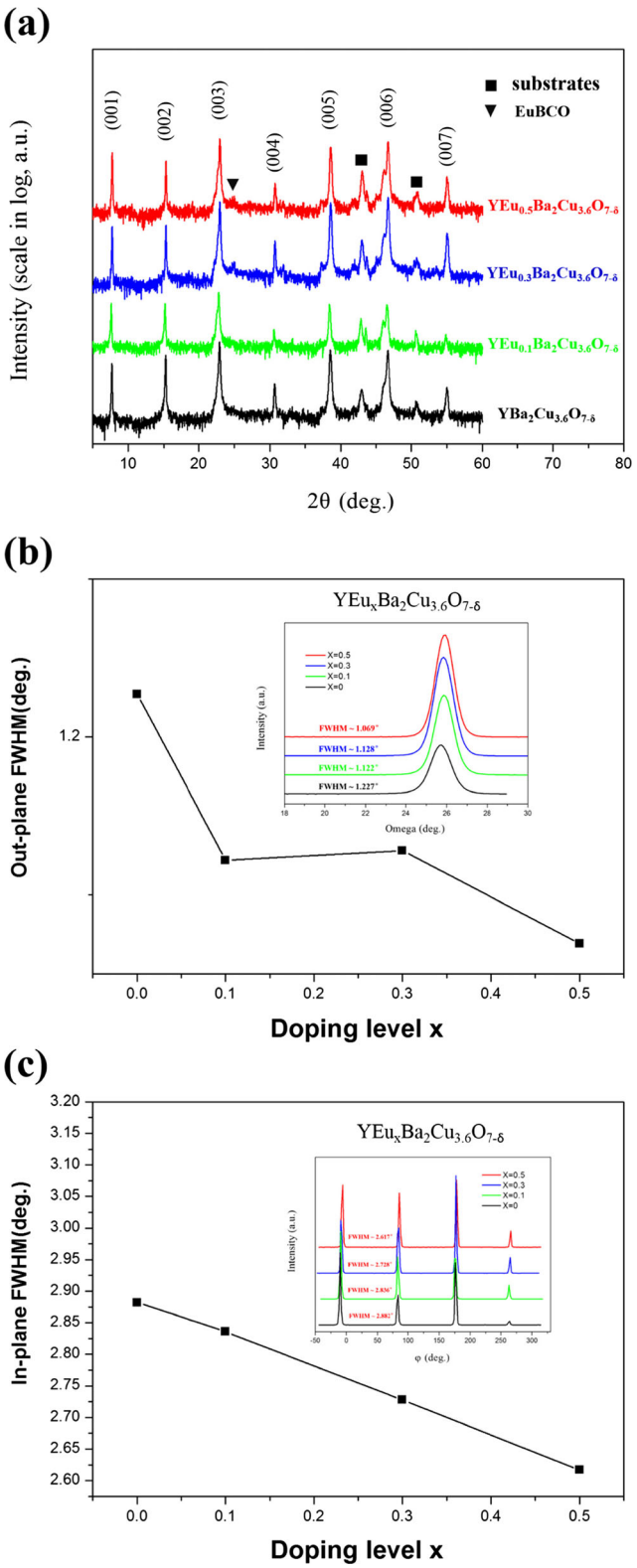


**Fig. 1** **a** Typical $\theta$–$2\theta$ x-ray diffraction patterns of pure and Eu-doped YBCO films with different doping levels. **b** The FWHM values based on (006) omega-scan and **c** (103) phi-scan rocking curves of pure and Eu-doped YBCO films

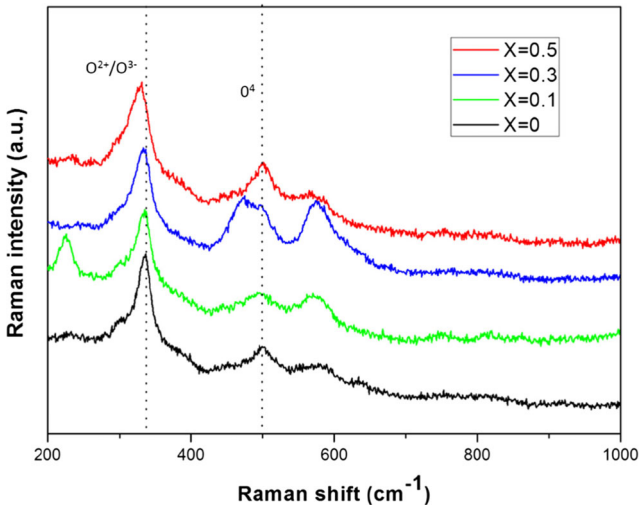


**Fig. 2** Raman spectra of pure and Eu-doped YBCO films with different doping levels

followed by a crystallization process in flowing atmosphere of humid oxygen/nitrogen mixture. Finally, the as-grown thin films were annealed at 450° in flowing oxygen for 60 min.

The Empyrean x-ray system was used to record the $\theta$–$2\theta$XRD patterns, which characterized the phase purity of the films. The texture analyses including $\omega$-scan and $\varphi$-scan were performed using the Empyrean x-ray equipped with a fourcrystal monochromator. Raman spectroscopy (INVIA) is used to verify the $c$-axis grains are dominant. The microstructure analyses were performed by field-emission scanning electronic microscopy (FE-SEM) which is also utilized to get further information of surface morphology. Energy-dispersive spectroscopy (EDS) was applied as the preferred method to identify the presence of elements and their composition. Spatial distribution of the $J_c$ value was obtained by mapping analysis of inductive measurement by self-field at 77 K. The superconducting properties under magnetic fields were measured by magnetic property measurement system with a SQUID magnetometer. The $J_c$ value of the films at 70 K was determined by the Bean critical state model formula using the M–H curve.

## 3 Results and Discussion

Figure 1a shows the x-ray diffraction $\theta$–$2\theta$ patterns of Eu-doped YBCO films with $x = 0$, 0.1, 0.3, and 0.5. As it can be seen all derived thin films are in (00$l$) orientation, indicating that all thin films show well $c$-axis orientation. In addition, we can detect the EuBCO phase at about 25° when doping Eu element.

In order to further examine the texture, $\omega$-scan and $\varphi$-scan rocking curves have been documented in Fig. 1b, c. The typical $\omega$-scan rocking curves of pure and Eu-doped

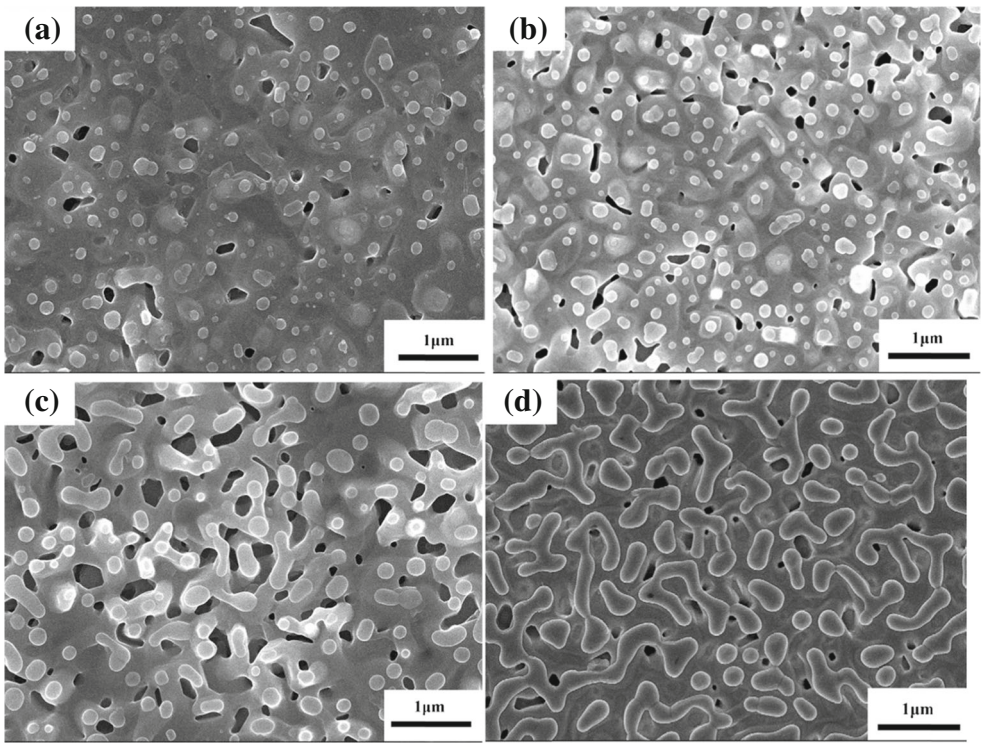


**Fig. 3** SEM micrographs of **a** pure and **b** Eu-doped YBCO films with $x = 0.1$, **c** $x = 0.3$ and **d** $x = 0.5$

films around the (006) peak are performed in Fig. 1b to estimate the quality of out-of-plane alignment. The full width at half maximum (FWHM) of (006) peak are 1.227°, 1.122°, 1.128°, and 1.069° for $YBa_2Cu_{3.6}O_{7-\delta}$, $YEu_{0.1}Ba_2Cu_{3.6}O_{7-\delta}$, $YEu_{0.3}Ba_2Cu_{3.6}O_{7-\delta}$ and $YEu_{0.5}Ba_2Cu_{3.6}O_{7-\delta}$ films respectively showing the good out-of-plane alignment. Figure 1c shows the $\varphi$-scan curve of (103) face of the films, and the FWHM are 2.882°, 2.836°, 2.728° and 2.617° respectively, which indicates the good in-plane alignment. The results demonstrate the successful preparation of biaxially textured Eu-doped and pure YBCO films. In addition, it also reveals the better out-of-plane and in-plane alignment when adding Eu element.

Figure 2 shows the results of Raman microprobe measurements on the pure and Eu-doped YBCO films with different doping levels. As previously pointed out, the presence of both the $O^{2+}/O^{3-}$ out-of-phase mode and the $O^4$ mode in the same scattering geometry signifies the presence of both $c$-axis and $a$-axisoriented grains. If $I_{O2+/O3-}/I_{O4} > 1$, the formula suggests that the $c$-axis grains are dominant. In the case of films such as $I_{O2+/O3-}/I_{O4} < 1$, the formula suggests that the $a$-axis grains are dominant. As is shown in the graph, all the $O^4$ modes are very weak, the films show main $c$-axis growth which is consistent with $x$-ray $\theta$–$2\theta$.

Figure 3a–d show the surface morphologies of pure and Eu-doped YBCO films with different doping levels. It can be seen that the surface morphologies are smooth in density and crack-free. Meanwhile, many special nanoparticles and solid holes can be found on the surface of Eu-doped YBCO films, which is different from the case in pure YBCO graph. Besides, these nanoparticles are regularly scattered across the film surface. The dimensions of the particles on the Eu-doping film are larger than the pure YBCO films. Based on the above analysis, the presence of these nanoparticles and solid holes are probably due to the formation of EuBCO phase. In order to further observe the surface structure, AFM images of $YBa_2Cu_{3.6}O_{7-\delta}$ and $YEu_{0.5}Ba_2Cu_{3.6}O_{7-\delta}$ thin films had been obtained As shown in Fig. 4, the $YEu_{0.5}Ba_2Cu_{3.6}O_{7-\delta}$ thin film tends to be more smooth and regular than the pure $YBa_2Cu_{3.6}O_{7-\delta}$ film.

The compositions and elements ratio of these particles on the $YEu_{0.3}Ba_2Cu_{3.6}O_{7-\delta}$ film surface are determined by EDS spectra. It is found that the nanoparticles in the film contain Eu in Fig. 5a. Moreover, the distributions of europium are uniform rather than clustered together. The element content on the surface of the $YEu_{0.3}Ba_2Cu_{3.6}O_{7-\delta}$ film is in accordance with the original stoichmetric ratio as given in Fig. 5b.

Typical results of the temperature dependence of magnetization for pure and Eu-doped YBCO films are shown in Fig. 6. As can be seen, all the films show relatively small superconducting transition width, elucidating the existence of pure and homogeneous superconducting phase. And the

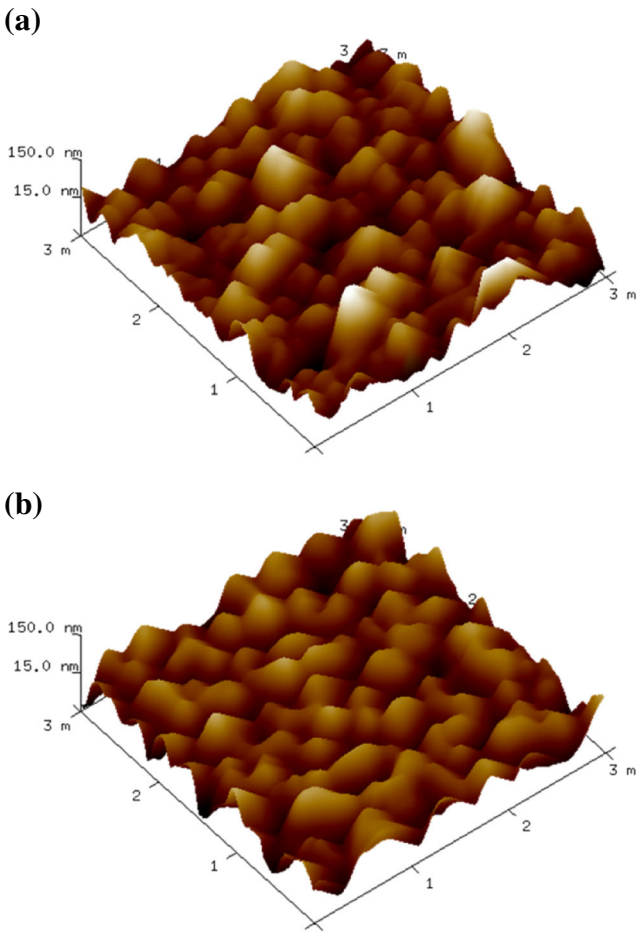


**Fig. 4** AFM images of the **a** $YBa_2Cu_{3.6}O_{7-\delta}$ and **b** $YEu_{0.5}Ba_2Cu_{3.6}O_{7-\delta}$ thin films

superconducting transition width tends to decrease with the doping levels which indicates the europium doping into the YBCO film. In addition, the critical temperatures improve with increasing doping levels (see in the inset of Fig. 6). X-ray diffraction analyses reveal the presence of amounts of EuBCO phase with relatively higher $T_c$ and Eu doping will increase the concentration of the hole carriers in Eu-doped YBCO films, which may be cooperatively responsible for the improved $T_c$ with the doping levels. Figure 7 shows inductive $J_c$ mapping graphs of specimens deposited on pure and Eu-doped YBCO films with different doping levels at 77 K. The average and maximum $J_c$ values of $YEu_{0.3}Ba_2Cu_{3.6}O_{7-\delta}$ were 2.29 and 2.52 MA/cm$^2$, respectively, which are higher than the other films. The data indicates that $J_c$ of the superconductor films improved with europium addition.

As can be seen in Fig. 8, YBCO film with $x = 0.3$ displays the best $J_c$–H behavior at low-field. But the $J_c$ of $YEu_{0.3}Ba_2Cu_{3.6}O_{7-\delta}$ is lower than the $YEu_{0.5}Ba_2Cu_{3.6}O_{7-\delta}$ film above 0.2 T at 70 K. Even so,

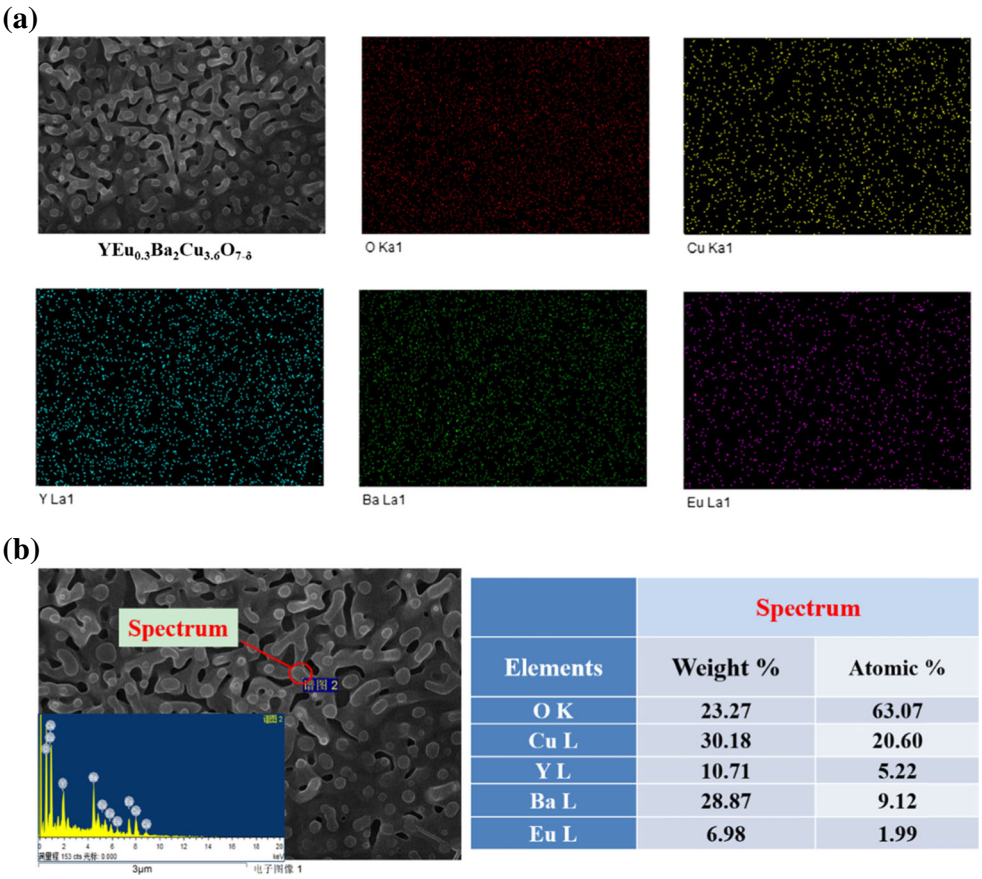


| | Spectrum | |
|---|---|---|
| Elements | Weight % | Atomic % |
| O K | 23.27 | 63.07 |
| Cu L | 30.18 | 20.60 |
| Y L | 10.71 | 5.22 |
| Ba L | 28.87 | 9.12 |
| Eu L | 6.98 | 1.99 |

**Fig. 5** **a** EDS maps of Y, Ba, Cu, O, and Eu elements on the surfaces of $YEu_{0.3}Ba_2Cu_{3.6}O_{7-\delta}$ film (color online). **b** EDS spectra of point scanning on the $YEu_{0.3}Ba_2Cu_{3.6}O_{7-\delta}$ films in order to confirm the element content

the films with Eu addition have a higher $J_c$–H property than that of pure film in all fields. The above results suggest that the $J_c$–H behavior can be remarkably enhanced by Eu doping in YBCO films.

The mechanism for the remarkable improvement of critical current density can be explained by the improved microstructure and quite strong flux pinning in Eu-doped YBCO films. As revealed by microstructural analyses in Figs. 1 and 3, dilute Eu doping of YBCO film leads to the smoother surface microstructure and good out-of-plane and in-plane alignment. This means Eu doping plays an important role in enhancing the epitaxial growth of YBCO films. Besides, Eu doping to YBCO will result in the lattice

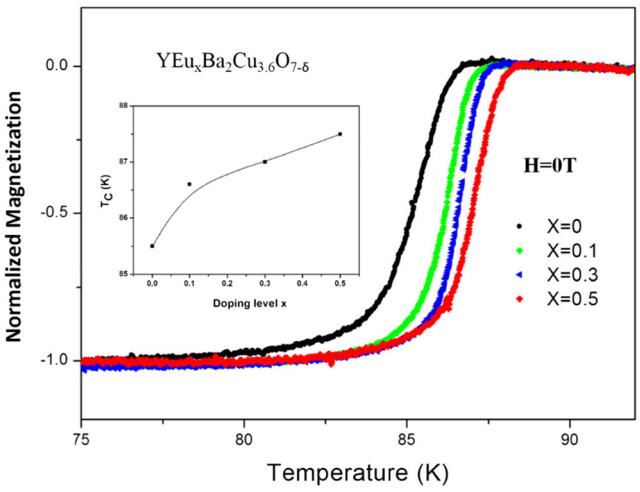


**Fig. 6** Temperature dependence of magnetization for pure and Eu-doped YBCO films with different doping levels. *Inset* is the Eu doping level dependence of $T_c$

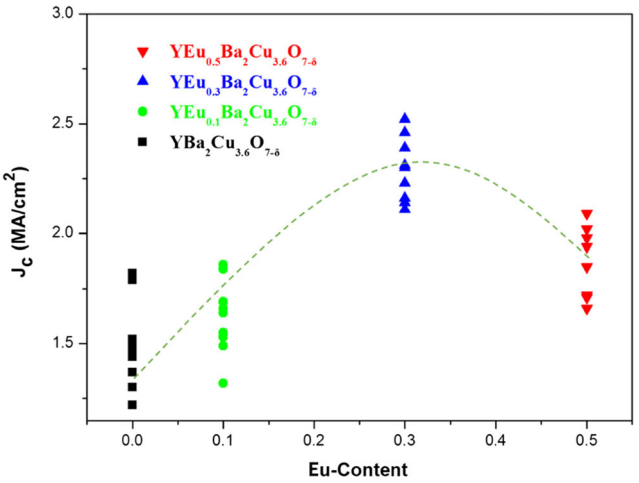


**Fig. 7** Inductive $J_c$ mapping graphs of specimens deposited on pure and Eu-doped YBCO films with different doping levels at 77 K

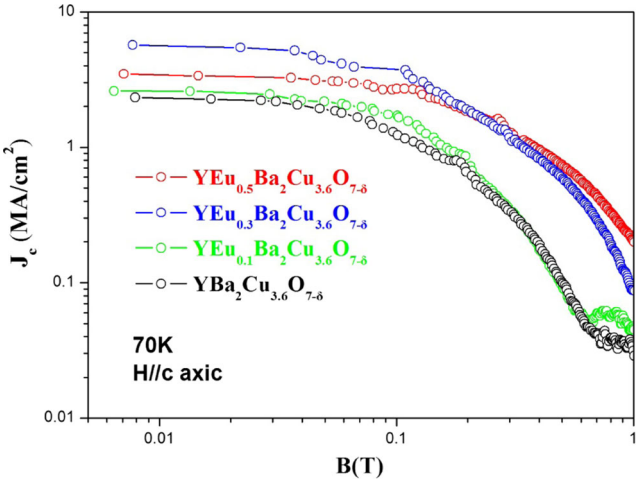


**Fig. 8** Magnetic field dependence of $J_c$ for pure and Eu-doped YBCO films at 70 K

deformation because of different ionic radius. As a result, the superconductivity was locally suppressed by the oxygen vacancies through the lattice deformation. Therefore, the lattice deformation introduced by Eu doping is suggested to act as the effective pinning centers in Eu-doped YBCO films.

To better understand the essential Eu-doping effect on flux pinning properties of YBCO films, it is necessary to make further studies such as transmission electron microscopy observation and transport measurements. Additionally, detailed researches like the influence of different doping elements on flux pinning properties of YBCO films were carried out in our group.

## 4 Conclusion

Biaxially textured pure and Eu-doped YBCO films about 400 nm were prepared on buffered substrates by TFA-MOD method Eu-doped YBCO films showed better out- and in-plane texture and exhibited the special morphology. The $T_c$ and diamagnetic signal increase with the doping levels. The in-filed $J_c$ values are significantly improved by Eu doping with $x = 0.1$, 0.3 and 0.5, and the film with $x = 0.3$ has the best performance by self-filed and in low-field. However, the $J_c$–H behavior for film with $x = 0.5$ is better than $x = 0.3$ above 0.2 T at 70 K. The high performance of Eu-doped YBCO films can be explained by the good grain connections as well as the effective flux pinning centers introduced by Eu doping. These results indicate that Eu doping is a perspective way to essentially improve the current carrying capability of YBCO films.

**Acknowledgments** This work was supported in part by Shanghai Key Laboratory of High Temperature Superconductors (14DZ2260700); the Science and Technology Commission of Shanghai Municipality (16521108400, 16DZ0504300 and 14521102800), the National Natural Science Foundation of China (51572165, 11174193 and 51202141).

## References

1. Wang, W.T., Yang, X.F., Pu, M.H., Zhang, H., Cheng, C.H., Zhao, Y.: Influence of Heat treatment on structure and superconducting properties of YBCO film by chemical solution deposition method. J. Supercond. Nov. Magn. **25**, 39–44 (2011)
2. Wang, W.T., Wang, Z., Pu, M.H., Wang, M.J., Zhang, X., Lei, M., Zhao, Y.: A novel partial melting process for YBa2Cu3O7-z superconducting films by fluorine-free polymer-assisted metal organic deposition approach. J. Supercond. Nov. Magn. **28**, 3249–3253 (2015)
3. Shin, H.-S., Gorospe, A., Bautista, Z., Dedicatoria, M.J.: Evaluation of the electromechanical properties in GdBCO coated conductor tapes under low cyclic loading and bending. Supercond. Sci. Technol. **29**, 014001 (2016)
4. Senatore, C., Barth, C., Bonura, M., Kulich, M., Mondonico, G.: Field and temperature scaling of the critical current density in commercial REBCO coated conductors. Supercond. Sci. Technol. **29**, 014002 (2016)
5. Kesgin, I., Khatri, N., Liu, Y., Delgado, L., Galstyan, E., Selvamanickam, V.: Influence of superconductor film composition on adhesion strength of coated conductors. Supercond. Sci. Technol. **29**, 015003 (2016)
6. Liu, Y., Du, G.: Preparation and flux-pinning properties of multilayered yttrium barium copper oxide thin films containing alternating barium zirconate and yttria nanostructures. J. Electron. Mater. **40**, 1512–1516 (2011)
7. Maiorov, B., Wang, H., Foltyn, S.R., Li, Y., DePaula, R., Stan, L., Arendt, P.N., Civale, L.: Influence of naturally grown nanoparticles at the buffer layer in the flux pinning in YBa2Cu3O7 coated conductors. Supercond. Sci. Technol. **19**, 891–895 (2006)
8. Aytug, T., Paranthaman, M., Gapud, A.A., Kang, S., Christen, H.M., Leonard, K.J., Martin, P.M., Thompson, J.R., Christen, D.K., Meng, R., Rusakova, I., Chu, C.W., Johansen, T.H.: Enhancement of flux pinning and critical currents in YBa2Cu3O7-$\delta$ films by nanoscale iridium pretreatment of substrate surfaces. J. Appl. Phys. **98**, 114309 (2005)
9. Zhang, H.L., Ding, F.Z., Gu, H.W., Dong, Z.B., Qu, F., Shang, H.J.: Effect of Ba/Y molar ratio on superconducting properties of BaTiO3-Doped YBa2Cu3O7-$\delta$ Films. J. Supercond. Nov. Magn. **29**, 1227–1232 (2016)
10. Wang, H.-Y., Ding, F.-Z., Gu, H.-W., Zhang, H.-L., Dong, Z.-B.: Microstructure and superconducting properties of (BaTiO3, Y2O3)-doped YBCO films under different firing temperatures. Rare Metals (2015)
11. Sandu, V., Aldica, G., Liu, Z.Y., Zhang, Z.L., Suo, H.L.: Effect of silver addition to superconducting SmFeAsO1-xFx. J. Supercond. Nov. Magn. **27**, 1635–1641 (2014)
12. Wang, F.: Superconducting properties enhancement of YBa2Cu3O7-$\delta$ thin films by BaSnO3 doping. J. Mater. Sci.: Mater. Electron. (2016)
13. Guo, P., Zhao, X.-H., Xiong, J., Liu, X.-Z., Tao, B.-W.: Polymer assisted thick single-layer YBa2Cu3O7-$\delta$ films prepared with modified TFA-MOD method. Rare Metals **33**, 594–597 (2014)

14. Yokoe, D., Kato, T., Tobita, H., Ibi, A., Yoshizumi, M., Izumi, T., Hirayama, T., Shiohara, Y.: Transmission electron microscopy study of GdBa2Cu3O7-x containing nano-sized BaMO3 (M: Hf, Zr, Sn) rods fabricated by pulsed laser deposition. J. Mater. Sci. **48**, 125–131 (2012)
15. Peng, L., Liu, Y., Gao, T., Cai, C., Zhang, J.: Vortex activation energy and normalized magnetization relaxation rate in the YBa2Cu3O7-δ/YSZ quasi-multilayer. J. Supercond. Nov. Magn. **24**, 1683–1686 (2010)
16. Miura, S., Yoshida, Y., Ichino, Y., Matsumoto, K., Ichinose, A., Awaji, S.: Flux pinning properties of a SmBa2Cu3Oy film including high number density of BaHfO3 nano-rods on LaAlO3 substrate. J. Supercond. Nov. Magn. **28**, 367–369 (2014)
17. Strickland, N.M., Long, N.J., Talantsev, E.F., Hoefakker, P., Xia, J., Rupich, M.W., Kodenkandath, T., Zhang, W., Li, X., Huang, Y.: Enhanced flux pinning by BaZrO3 nanoparticles in metal-organic deposited YBCO second-generation HTS wire. Physica C: Superconductivity **468**, 183–189 (2008)
18. Wong-Ng, W., Yang, Z., Cook, L.P., Frank, J., Loung, M., Huang, Q.: Phase equilibria of BaO-R2O3-CuOz systems (R = Y and lanthanides) under CO2-free conditions. J. Electron. Mater. **36**, 1279–1287 (2007)
19. Badea, C., Mos, R.B., Ciontea, L., Ardelean, I.: Low-field nuclear magnetic resonance relaxometry as a tool in monitoring the aging of coating solutions (case study: barium propionate precursor coating solution). Appl. Magn. Reson. **39**, 365–372 (2010)
20. Jin, L.H., Lu, Y.F., Feng, J.Q., Yu, Z.M., Wang, Y., Li, C.S.: Fabrication of YBCO film using a new copper precursor by chemical solution method. J. Supercond. Nov. Magn. **25**, 1695–1699 (2012)